Chemistry–A European Journal
Research Article
doi.org/10.1002/chem.202404468
Chemistry Europe
European Chemical Societies Publishing
www.chemeurj.org

An Oxoiron(IV) Complex Supported by an N-Alkylated Cyclam Ligand System Containing a Pendant Alcohol Moiety

Dibya Jyoti Barman,[a] Thomas Lohmiller,[a, b] Sagie Katz,[c] Michael Haumann,[d] Peter Hildebrandt,[c] Wonwoo Nam,*[e] and Kallol Ray*[a]

The effect of a pendant neutral alcohol moiety in the N-alkylated cyclam (1,4,8,11-tetraazacyclotetradecane) ligand backbone is examined for the non-heme mononuclear oxoiron(IV) unit in $[Fe^{IV}(O_{syn})(TMC\text{-}HOR)(NCCH_3)]^{2+}$ (**1-*syn***) (TMC-HOR = 2-(4,8,11-trimethyl-1,4,8,11-tetraazacyclotetradecan1-yl)ethan-1-ol). Unlike in the related $[Fe^{IV}(O_{anti})(TMC\text{-}SR)]^{+}$ (**3-*anti***) (TMC-SR = 1-mercaptoethyl-4,8,11-trimethyl-1,4,8,11-tetraazacyclotetradecane) complex, bearing an axial mono-anionic thiolate ligand *trans* to the oxo unit, the alcohol moiety in **1-*syn*** stays protonated and does not axially coordinate to iron. The protonation of the alcohol moiety is a prerequisite for the stabilization of the oxoiron(IV) core; it presumably serves as a hydrogen bonding donor to the oxoiron(IV) unit, which is positioned *syn* to the three methyl groups. Comparative reactivity studies reveal **1-*syn*** to be a stronger hydrogen atom abstraction but weaker oxygen atom transfer agent relative to the $[Fe^{IV}(O_{syn})(TMC)(NCCH_3)]^{2+}$ (**2-*syn***) complex, bearing the *N*-tetramethylated cyclam (TMC) ligand.

Introduction

In biology, dioxygen is often activated at heme and non-heme iron centers to carry out important and diverse oxidative transformations.[1] High-valent oxoiron(IV) species are frequently invoked as reactive oxidants in these reactions.[1a] Driven by the need to understand the fundamental properties of such oxoiron(IV) centers and to exploit their oxidative capabilities[1b] in unprecedented organic transformations, a relatively large family of oxoiron(IV) complexes[2] has been synthesized and comprehensively characterized, the vast majority of which exhibit an intermediate spin ($S = 1$) state.[3] This is in contrast to the oxoiron(IV) moieties in enzymes,[4] all of which have been found in the quintet ($S = 2$) spin state. Furthermore, in contrast to nature, where -O atom donors are ubiquitous, most of the biomimetic oxoiron(IV) complexes are stabilized by employing strong-field pyridine,[5] tertiary amine[6] or carbene donors.[6–7]

Electronic effects[1b,8] on the reactivity of oxoiron(IV) complexes have been investigated[9] in significant detail. Theoretical studies[10] have rationalized a much higher hydrogen atom abstraction (HAA) reactivity of the naturally occurring $S = 2$ oxoiron(IV) complexes compared to $S = 1$. This is mainly because of the linear transition state involving a σ attack of the substrate with the dz^2 orbital of the metal, which provides a lower steric contribution to the barrier at the transition state for the $S = 2$ surface.[11] In contrast, the π attack required for the reactivity on the $S = 1$ surface is sterically hindered, which results in a large barrier at the transition state and depleted reactivity. The unexpectedly high reactivity observed in some of the model $S = 1$ oxoiron(IV) complexes has, therefore, been explained by a two-state reactivity (TSR) model,[12] where the $S = 1$ oxoiron(IV) core tunnels into the low-lying $S = 2$ transition state for HAA reactivity. For example, TSR is reflected in the anti-electrophilic reactivity pattern of a series of complexes[13] $[Fe^{IV}(O_{anti})(TMC)(X)]^{n+}$ (n = 2: X=$NCCH_3$ (**2-*anti***, Scheme 1); n = 1: X=$O_2CCF_3^-$, N_3^-) and $[Fe^{IV}(O_{anti})(TMC\text{-}SR)]^{+}$ (**3-*anti***) with dihydroanthracene. Introducing a stronger electron donating axial ligand led to a decrease in the calculated energy gap (ΔE_{TQ}) between the triplet ground state and the quintet excited state, which lowered the activation barrier for HAA, because of the better accessibility[13] of the more reactive $S = 2$ state. The replacement of one of the equatorial NMe donors in TMC by an O-atom in TMCO (TMCO = 4,8,12-trimethyl-1-oxa-4,8,12-triazacyclotetradecane) also led to a decrease in ΔE_{TQ}, thereby transforming the sluggish complex, **2-*anti***[2b,14] into a highly reactive oxidant, $[Fe^{IV}(O_{anti})(TMCO)(OTf)]^{+}$. The observed high HAA

[a] D. Jyoti Barman, T. Lohmiller, K. Ray
Department of Chemistry, Humboldt-Universität zu Berlin, Brook-Taylor-Straße 2, 12489 Berlin, Germany
E-mail: kallol.ray@chemie.hu-berlin.de
[b] T. Lohmiller
EPR4Energy Joint Lab, Department Spins in Energy Conversion and Quantum Information Science, Helmholtz-Zentrum Berlin für Materialien und Energie GmbH, Albert-Einstein-Str. 16, 12489 Berlin, Germany
[c] S. Katz, P. Hildebrandt
Department of Chemistry, Technische Universität Berlin, Straße des 17. Juni 135, 10623 Berlin, Germany
[d] M. Haumann
Department of Physics, Freie Universität Berlin, Arnimallee 14, 14195 Berlin, Germany
[e] W. Nam
Department of Chemistry and Nano Science, Ewha Womans University, Seoul 03760, Korea
E-mail: wwnam@ewha.ac.kr

Supporting information for this article is available on the WWW under https://doi.org/10.1002/chem.202404468

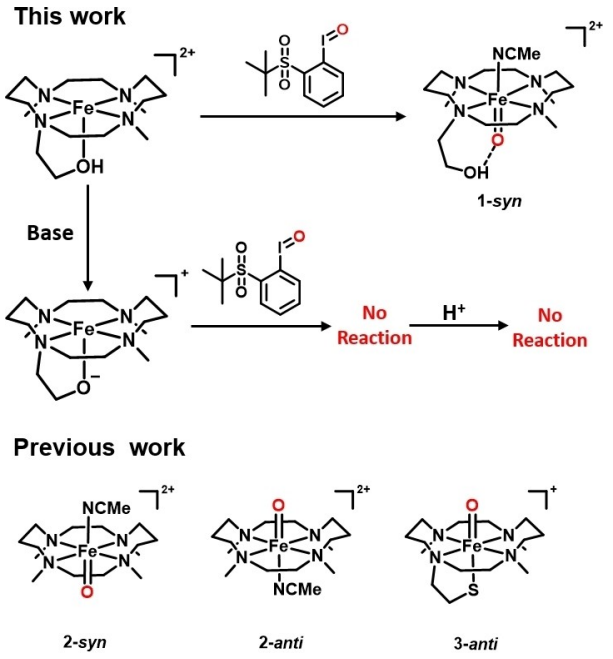

Scheme 1. Schematic representation of the oxoiron(IV) intermediates.

reactivities of **3-*anti*** [14] and $[Fe^{IV}(O_{anti})(TMCO)(OTf)]^{+}$ [2b] provide a compelling rationale for nature's use of the O=Fe^{IV}–SR motif [15] and weak-field O-based ligands in heme and non-heme oxygenases, [16] respectively, to perform key metabolic transformations that involve the activation of strong C–H bonds.

In our continuing efforts to uncover the structure–reactivity relationships of non-heme metal-oxo complexes, herein we investigate how alcohol coordination influences the reactivity of the oxoiron(IV) unit. Although phenol-ligated iron(IV)-oxo centers are postulated to be the key oxidants in the catalytic cycles of catalase enzymes, [15f,17] an appropriate model complex is lacking in the literature. Based on the reported stabilization of **3-*anti***, where the oxo group binds *anti* to the three –Me and $–CH_2–CH_2–S^-$ groups of the TMC-SR ligand, we reasoned that appending an alcohol donor to the ligand framework would also promote coordination of the deprotonated alcohol ligand to the iron(IV) center. This was tested by replacing one of the methyl substituents of TMC by a $–CH_2–CH_2–OH$ group, affording the ligand TMC-HOR, which stabilizes the corresponding oxoiron(IV) moiety in **1-*syn*** (Scheme 1). Surprisingly, TMC-HOR stays protonated; DFT calculations and ^{1}H-NMR analysis suggest a H-bonding interaction between $–CH_2CH_2OH$ and the oxoiron(IV) moietiy. The stabilization of a hydrogen bonded Fe^{IV}=O_{syn}-HOR moiety in **1-*syn***, in contrast to the deprotonated thiolate RS–Fe^{IV}=O_{anti} core in **3-*anti***, improves our understanding of the effect of $–S^-$ vs. –OH donors to form the oxoiron(IV) core in an otherwise identical ligand framework.

Results and Discussion

The neutral ligand, **TMC**-HOR with a pendant alcohol moiety in focus was synthesized in moderate yield according to a previously reported procedure. [19] Combination of the **TMC**-HOR ligand with $Fe(OTf)_2(CH_3CN)_2$ in acetonitrile resulted in the expected iron(II) complex, $[Fe^{II}(TMC\text{-}HOR)](CF_3SO_3)_2$ (see ESI, synthesis section and Figure S1), with 99% yields.

The X-ray diffraction (XRD) analyzed structure (Figure 1) of $[Fe^{II}(TMC\text{-}HOR)](CF_3SO_3)_2$ displays a 5-coordinate geometry with a structural parameter (τ_5) [20] *value of* 0.48, which is in between square pyramidal and trigonal bipyramidal geometries. The N-alkylated cyclam ring exhibits a *trans*-I configuration, [21] similar to that seen in all previously reported X-ray structures of iron(II) TMC complexes, [3a,9,18,21–24c] and the appended $–CH_2CH_2OH$ donor coordinates to the iron center *via* its O-atom in a protonated state. Interestingly, the alcohol moiety is H-bonded to one of the triflate anions. The XRD-determined iron-ligand bond lengths (Table S1) associated with $[Fe^{II}(TMC\text{-}HOR)](CF_3SO_3)_2$ are characteristic of a 5-coordinate high-spin iron(II) complex, with an average Fe–N distance of 2.1627(19) Å and an Fe–O bond of 2.0511(16) Å.

Mössbauer spectroscopy further confirmed the presence of an $S=2$ Fe^{II} center in $[Fe^{II}(TMC\text{-}HOR)](CF_3SO_3)_2$ with a quadrupole splitting (ΔE_Q) of 3.51 mm/s and an isomer shift (δ) of 0.98 mm/s (Figure 2, top). As the Mössbauer parameters of $[Fe^{II}(TMC\text{-}HOR)]^{2+}$ are similar to those reported for the $[Fe^{II}(TMC\text{-}SR)]^{+}$ complex ($\Delta E_Q = 3.0$ mm/s and $\delta = 0.90$ mm/s), [22h] -S vs -OH binding has only a minor influence on the electronic structure of the high-spin Fe^{II} state.

Reaction of $[Fe^{II}(TMC\text{-}HOR)](CF_3SO_3)_2$ with 1.2 equivalents of 2-(*tert*-butylsulfonyl)iodosylbenzene ($^tBuSO_2C_6H_4IO$, sPhIO) in CH_3CN at −40 °C gave a bright yellow colored solution of a new species, **1-*syn*** (half-life ($t_{1/2}$) of 7 minutes at 25 °C), exhibiting an electronic spectrum with a near-infrared (NIR) absorption band ($\lambda_{max} = 820$ nm; $\varepsilon_{max} = 320\ M^{-1}\ cm^{-1}$) characteristic of $S=1$ oxoiron(IV) complexes (Figure 3, Table 1). [24a] Previously, features of this type have been assigned to ligand field transitions arising from an $S=1$ oxoiron(IV) center, with the accompanying well-defined fine structures being vibronic in nature. [22–24c]

Notably, relative to **3-*anti***, the NIR band of **1-*syn*** is blue-shifted with increased absorption intensity (Table 1), which is consistent with the strong axial donation of the anionic -S^-R group in **3-*anti***. On the basis of detailed magnetic circular dichroism (MCD) studies, [9] these spectral changes have been

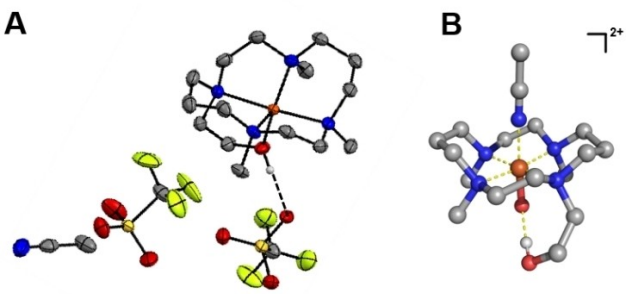

Figure 1. (A) XRD determined molecular structure of $[Fe^{II}(TMC\text{-}HOR)](CF_3SO_3)_2].CH_3CN$, showing unbound triflate anions and a co-crystallized acetonitrile solvent molecule. Hydrogen atoms (except at OH of the TMC-HOR ligand) are omitted for clarity. Ellipsoids are drawn at 50% probability level. (B) DFT optimized structure of **1-*syn***.

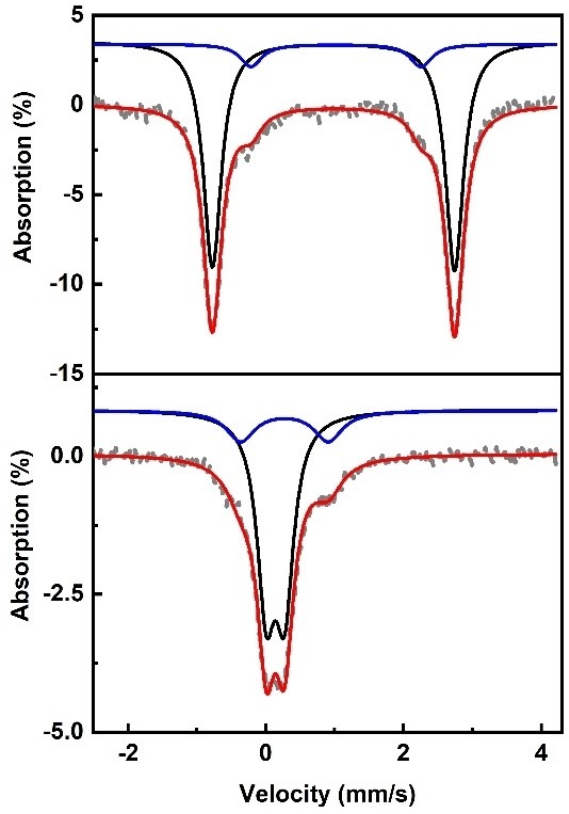

Figure 2. Mössbauer spectra of a powder sample of $[Fe^{II}(TMC\text{-}HOR)](CF_3SO_3)_2$ (top) and of a frozen CH_3CN solution of **1-*syn*** (bottom) recorded at 14 K (experimental data, grey dashed lines; fitted curves, red solid lines; major and minor species are shown by black and blue solid lines, respectively).

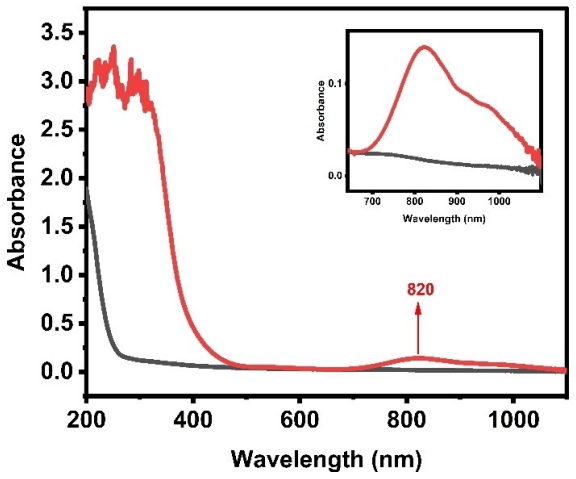

Figure 3. UV-vis spectral changes associated with the formation of ***1*-syn** (red) by reacting $[Fe^{II}(TMC\text{-}HOR)](CF_3SO_3)_2$ (1 mM, black) in CH_3CN at −40 °C with 1.2 eq sPhIO. The inset shows an expansion of the NIR region.

attributed to perturbations in Fe=O π-interactions caused by the *trans* ligand. Interestingly, the axial donation in **2-*syn*** (λ_{max} = 815 nm) and **2-*anti*** (λ_{max} = 824 nm), containing a neutral CH_3CN ligand, is very similar to **1-*syn***, as evident from the similar λ_{max} values (Table 1), which may point towards axial CH_3CN donation instead of a neutral -ROH in **1-*syn***.

The ^{1}H NMR spectrum of **1-*syn*** (Figure 4), acquired in acetonitrile-d_3 at −40 °C, provides further structural insights. The sharp peaks corresponding to the N–CH_3 groups are found in downfield region of the NMR spectrum around 30 ppm, but are separated due to their non-equivalent character. The α-CH_2 groups next to the amine -N donors appear as nine broad peaks of low intensity. All β-CH_2 groups reveal similar chemical shifts from 37 to 53 ppm, thereby confirming that the *trans*-I configuration is conserved in **1-*syn***, and also that the –CH_2–CH_2–OH ligand is not directly bound to the Fe^{IV} center, which would shift the β-CH_2 protons of –CH_2–CH_2–OH significantly. However, the two β-CH_2 protons of the pendant alcohol moiety appear as two separate peaks in **1-*syn***, which may indicate a locked conformation, presumably by H-bonding interaction with the oxoiron(IV) moiety. As per ^{19}F NMR (Figure S3), only one sharp signal at −79.90 ppm, corresponding to the free triflate anion, is observed, further corroborating acetonitrile as the axial ligand in **1-*syn***.

Mössbauer analysis of **1-*syn*** shows a doublet accounting for ~93% of the total iron with ΔE_Q = 0.25 mm/s and δ = 0.13 mm/s, which confirms the presence of an S = 1 iron(IV) center. Its electrospray mass spectrum exhibits an ion fragment at m/z = 357.1 (Figure S2), with a mass and isotope distribution pattern in agreement with its formulation as $[Fe^{IV}(^{16}O_{syn})(TMC\text{-}O^{-}R)]^+$ (calc. m/z 357.2). This ion peak shifts to m/z = 359.1 corresponding to $[Fe^{IV}(^{18}O_{syn})(TMC\text{-}O^{-}R)]^+$ (calc. m/z 359.2), when ^{18}O labelled sPhIO was used as an oxidant for the generation of the oxoiron(IV) species, **1-*syn***.

As a prerequisite for the stabilization of the oxoiron(IV) core in **1-*syn***, the TMC-HOR group needs to remain protonated. All efforts to generate the oxoiron(IV) species with the deprotonated $[Fe^{II}(TMC\text{-}OR)]^+$ complex failed.[24d] Addition of sPhIO to $[Fe^{II}(TMC\text{-}OR)]^+$ led to no change in the absorption spectrum in the near-IR region (Scheme 1). Thus, the *syn* site cannot be retrieved for oxo group transfer once the $[Fe^{II}(TMC\text{-}HOR)](CF_3SO_3)_2$ complex gets deprotonated. The significance of the protonated hydroxyl group in the TMC-HOR ligand system was further demonstrated in our attempt to isolate **1-*syn*** with the deuterated starting complex, $[Fe^{II}(TMC\text{-}DOR)](CF_3SO_3)_2$ (Figure S3), which also failed. This may corroborate the necessity of the H-bonding interaction in the stabilization of the Fe^{IV}=O moiety in **1-*syn***.

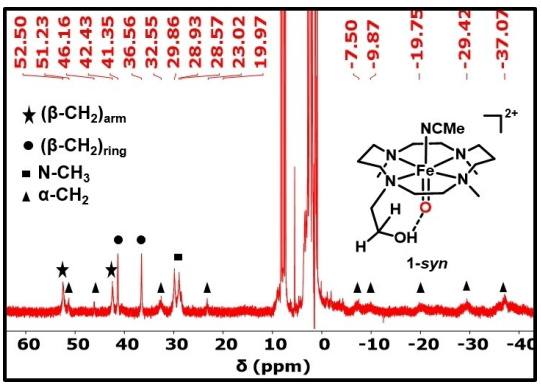

Figure 4. ^{1}H NMR spectrum of **1-*syn*** in acetonitrile-d_3 at −40 °C.

Table 1. Spectroscopic and structural properties of nonheme oxoiron(IV) complexes.

Complex	λ_{max} (nm) (ε (M^{-1} cm^{-1}))	δ (mm/s)	ΔE_Q (mm/s)	Fe=O (Å)	$\upsilon_{Fe=O}$ (cm^{-1})	$E_{K\text{-edge}}$ (eV)	Ref.
1-*syn*	820 (320)	0.13	0.25	1.65	862	7123.8	This work
2-*syn*	815 (380)	0.16	1.55	1.625	856	–	[24a]
2-*anti*	824 (400)	0.17	1.24	1.646	839	7124.5	[9]
3-*anti*	860 (230)	0.19	0.22	1.70	–	7125.3	[22 h]

Resonance Raman (rRaman) spectra (Figure 5) of **1-*syn*** using an excitation wavelength of 406 nm reveal the Fe=O vibrational mode at 862 cm^{-1}, which downshifts by 37 cm^{-1} upon introducing ^{18}O by the use of ^{18}O-labelled sPhIO (Figure 5), as expected for a diatomic Fe–O vibration (−38 cm^{-1}) based on Hooke's law.[24e] The related **2-*syn*** shows an Fe=O mode at 856 cm^{-1}, which is 6 cm^{-1} down-shifted compared to **1-*syn*** (Table 1). This slight difference in the Fe=O vibrational modes between **1-*syn*** and **2-*syn*** can likely be presumably attributed to presence of an additional pendant alcohol moiety in **1-*syn***, which leads to H-bonding interaction and different equatorial donation. A similar behavior of Fe=O vibrational modes with respect to H-bonding was previously reported in Hangman porphyrin complexes[26a] containing appended carboxylic, amide or ester groups,[3e,8g,25,26a] for all of which the Fe=O vibrational mode remained unchanged at 824 cm^{-1}. In these systems, the H-bonding donor site is covalently linked via a spacer group to the parent ligand backbone, which presumably reduces their flexibility and strength of the H-bonding to the Fe=O core. In contrast, a more flexible Fe^{IV}=O-H^+/LA (LA = lewis-acids)[26b] interaction (leading to stronger H-bonding interaction) in heme iron(IV)-oxo species resulted in a significant down-shift of the Fe=O vibrational mode compared to the respective non-hydrogen bonded system.

X-ray absorption spectroscopy (XAS) data were collected at the Fe K-edge for [Fe^{II}(TMC-HOR)](CF_3SO_3)$_2$ and **1-*syn***. The respective X-ray absorption near-edge structure (XANES) spectra are shown in Figure 6A. The K-edge energy of [Fe^{II}(TMC-HOR)](CF_3SO_3)$_2$ (7119.0 eV) indicates an iron(II) center (Table 1). The K-edge energy for **1-*syn*** (7123.8 eV) is lower relative to **3-*anti*** (7125.3 eV), presumably due to admixtures of iron(II) starting material and/or minor iron(III) oxidation products in the highly concentrated (15 mM) CH_3CN-solution sample of **1-*syn***, but consistent with previously reported values for **2-*anti*** (7124.5 eV)[14,18] and other oxoiron(IV) species (ca. 7124–7125 eV).[2] Complex **1-*syn*** exhibits a more prominent pre-edge transition compared to [Fe^{II}(TMC-HOR)](CF_3SO_3)$_2$ at ca. 7115 eV, as typical for oxoiron(IV) complexes and also observed for **2-*anti*** and **3-*anti***. It is noted that its broad envelope and relatively small amplitude in **1-*syn*** may suggest additional contributions from minor iron species in the sample.

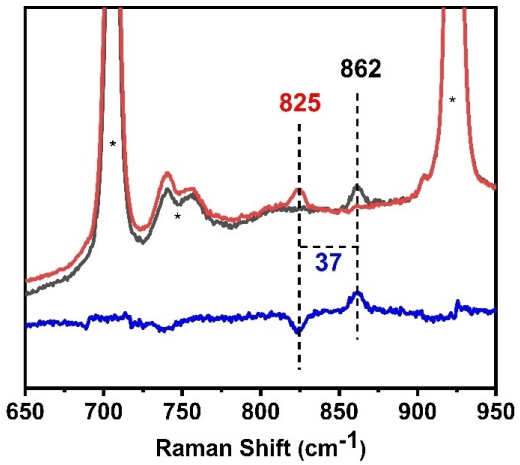

Figure 5. rRaman spectra of **1-*syn*** generated using sPhI^{16}O (black) and sPhI^{18}O (red) upon 406 nm excitation in CH_3CN at −40 °C. The blue line corresponds to the ^{16}O-^{18}O difference spectrum. (The asterisk marks solvent bands).

Extended X-ray absorption fine structure (EXAFS) spectra of [Fe^{II}(TMC-HOR)](CF_3SO_3)$_2$ and **1-*syn*** in frozen CH_3CN solution are shown in Figure 6B. Overall similar spectra imply that the ligand system remains intact upon oxidation. EXAFS simulation analysis (Table S2) for [Fe^{II}(TMC-HOR)](CF_3SO_3)$_2$ shows Fe–N bond lengths (~2.15 Å) in agreement with the crystal data and apparently resolves two further shorter iron-ligand bonds (~2.00 Å), likely due to the OH-group of the TMC-HOR ligand and a solvent (CH_3CN) molecule in *trans* position. The EXAFS parameters of **1-*syn*** (Table S2) reveal on average ca. 0.1 Å shortened Fe–N bonds and ca. 0.05 Å shortened second-sphere Fe–C distances upon iron oxidation. Slightly sub-stoichiometric amounts of an Fe=O bond of 1.65 Å were detected, as well as ca. one more oxygen/nitrogen ligand (~2.12 Å). These results are consistent with the replacement of the O atom of the pendant ROH moiety of the cyclic ligand by an oxo group at the ferryl center of **1-*syn***.

DFT computations were performed to verify the structural conformation of **1-*syn*** by comparison of bond distances and vibrational modes calculated for various geometry-optimized structures (Table S4) with the experimental results. The series of computational $S = 1$ state models comprises such structures in varying protonation states (i-iii) where the sPhIO derived O_{anti} donor atom replaces the coordinating CH_3CN in the *anti* position inferred from EXAFS for [Fe^{II}(TMC-HOR)](CF_3SO_3)$_2$, while the RO(H) moiety stays *trans*-coordinated, as well as structures (iv) where the oxo atom binds to the *syn* site, replacing the pendant ROH ligand, while CH_3CN remains *trans*. The O_{anti} structures exhibit on the *anti* and *syn* faces, respectively, (i) oxo and ROH, (ii) hydroxo and RO^- and (iii), in analogy to the thiolate-bound iron(IV)-oxo (**3-*anti***), oxo and RO^- ligands. All

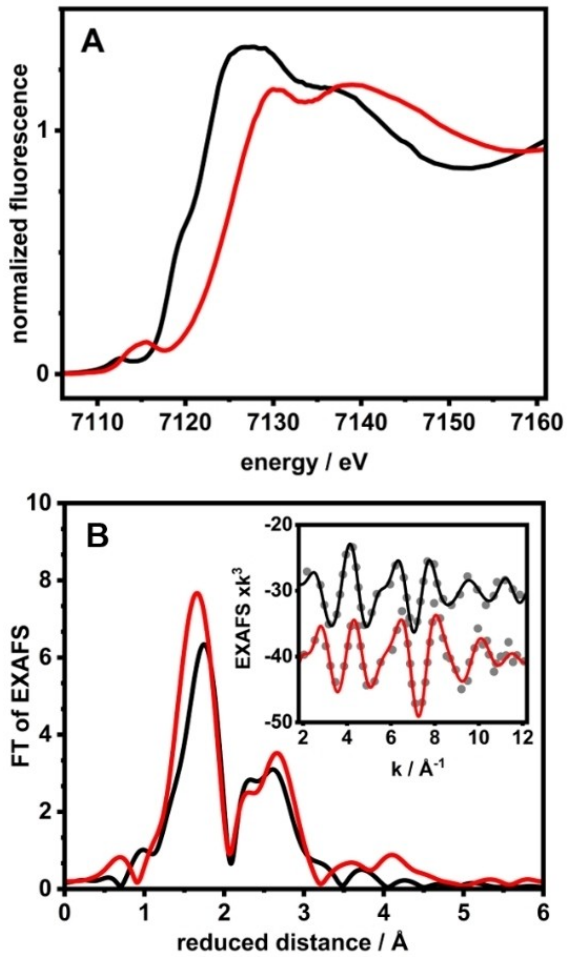

Figure 6. (A) Normalized Fe K-edge XANES spectra for [Fe^{II}(TMC-HOR)](CF$_3$SO$_3$)$_2$ (black) and **1-*syn*** (red) in frozen CH$_3$CN solution. (B) Fourier-transforms (experimental data) of the respective EXAFS spectra in the inset (experimental data, grey dotted line; simulations, thick black and red lines).

groups (i-iv) comprise two structures with different conformations of the *trans*–I TMC-HOR cycle, namely (a) as in **2-*syn*** and **2-*anti*** (C_s symmetry for TMC)[8,9, 21–24] and (b) as in iron(II) complexes with TMC-derived ligands (C_2 symmetry for TMC, see Figure 1 and Refs. [22–24]). In all cases, conformation b is lower in energy (by 1.6–4.2 kcal/mol), while all calculated properties are highly similar for a and b (Table S4).

For the oxo/ROH models (i), the $\nu_{Fe=O}$ vibration at 872–875 cm^{-1} ($\Delta^{18o-16o}\nu_{Fe=O} = -41$ cm^{-1}) deviates slightly from that experimentally determined by rRaman for **1-*syn*** (862 cm^{-1}, $\Delta^{18o-16o}\nu_{Fe=O} = -37$ cm^{-1}). In comparison, the hydroxo/RO$^-$ models (ii) are energetically favoured. However, the Fe–O distances of the latter approach similar values around 1.8 Å both for the weaker Fe-OH and the stronger Fe-$^-$OR bonds. Because of the nearly equidistant O ligands in *trans* positions, their Fe–O stretching vibrations couple to yield two modes, symmetric and antisymmetric, involving all three centers O–Fe-O at much lower energies of 557 and 646 cm^{-1}, respectively. Accordingly, compared to two-body Fe–O vibrations, their $^{16/18}$O isotope shifts are drastically reduced to −9–−10 cm^{-1}, which is inconsistent with the experiment. In the oxo/RO$^-$- models (iii), the calculated $\nu_{Fe=O} < 800$ cm^{-1} are also considerably too small compared to the experiment. In the CH$_3$CN/oxo models (iv), both the oxo and ROH moieties are located on the *syn* face, interacting via a H-bond of 1.65 Å length. The Fe=O and CH$_3$CN–Fe distances, as well as, the $\nu_{Fe=O}$ energies of 868–871 cm^{-1} ($\Delta^{18o-16o}\nu_{Fe=O} = -35$–37 cm^{-1} for **1-*syn***) are in excellent agreement with the experiment. Therefore, we prefer the structure shown in Figure 1B for **1-*syn***.

Reactivity Studies

The reactivity of **1-*syn*** was investigated in various HAA and OAT reactions and compared with those reported for **2-*syn*, 2-*anti*** and **3-*anti*** (Table 2). In each case, the pseudo-first-order reaction rates were monitored by the disappearance of the NIR absorption bands. The second-order rate constants (k_2) were calculated from the slope of a plot of the first-order rate constant (k_{obs}) versus substrate concentration (Figures S4–S8). The reactivity differences between **1-*syn*** and **2-syn** are also compared to check the effect of possible H-bonding on reactivity. Similar to that in the heme systems,[25,26] the presence of additional H-bonding effect in **1-*syn*** leads to enhanced HAA reactions, approximately by a factor of 2 compared to **2-*syn***. However, the OAT abilities of **1-*syn*** are significantly retarded relative to **2-*syn***. The KIE value of 11 (0 °C) for **1-*syn*** was determined using DHA-d_4 as a substrate. Polanyi curves for **1-*syn*** show a linear dependency of decreasing logarithmic effective reaction rates (k_2') with the increase of C–H BDE of the

Table 2. Second-order rate constants (k_2, M^{-1} s^{-1}) determined for C–H bond activation and OAT reactions of **1-*syn*** compared to those for the reported reactivity trend of **2-*syn***, **2-*anti*** and **3-*anti***.

Substrate	C–H BDE[a] (kcal/mol)	**1-*syn*** (25 °C) k_2 (M^{-1}s^{-1})	**2-*syn*** (25 °C)	**2-*anti*** (25 °C)	**3-*anti*** (0 °C)
Xanthene	75.50	1.64(5)	0.92	0.67	–
DHA	77	0.73(3)	0.33	0.23	7.50
CHD	78	0.70(2)	0.29	0.22	–
PPh$_3$	N/A	15.55*	too fast	29.5*	0.016

[a] Y.-R. Luo, Handbook of bond dissociation energies in organic compounds, CRC Press, New York, 2003. * These k_2 values are calculated for 25 °C from the experimentally determined value at 0 °C.

substrates. The value of the slope of −0.28 for **1-*syn***, implies that HAA is the rate-determining steps in all cases.

Under Ar atmosphere, the oxidations of xanthene and CHD by **1-*syn*** yielded xanthone (64%) and benzene (57%), respectively. Anthracene (7%), anthrone (5%) and anthraquinone (86%) products were obtained in reactions with dihydroanthracene (DHA). Complex **1-*syn*** also performed HAA with 2,4-di-tert-butylphenol to form 2,2'-dihydroxy-3,3',5,5'-tetra-tert-butylphenol (37%). In the event of OAT reaction, **1-*syn*** reacts with triphenylphosphine (PPh_3) to yield triphenylphosphine oxide (35%).

Conclusions

In summary, simply replacing the thiolate moiety with a neutral alcohol moiety, in the TMC-based ligand framework, leads to a substantially altered conformation of the non-heme oxoiron(IV) complex, thereby stabilizing an inverted CH_3CN-Fe^{IV}=O-HOR structure via H-bonding in **1-*syn***. In contrast, the thiolate ligated complex, **3-*anti***, stabilizes a deprotonated RS-Fe^{IV}=O core as a mimic of the cytochrome-P450 active center. The $-CH_2CH_2OH$ group of the TMC-HOR ligand needs to stay protonated as a prerequisite for the stabilization of the oxoiron(IV) moiety. A comparative reactivity study show an enhancement of HAA and reduction of OAT abilities of the H-bonded oxoiron(IV) core in **1-*syn*** compared to **2-*syn***. Surprisingly, however, a correlation of Fe=O bond strength and reactivity fails, as the H-bonded $\nu_{Fe=O}$ in **1-*syn*** appears at a slightly higher energy (862 cm^{-1}) relative to that in **2-*syn*** (856 cm^{-1}), despite of the higher HAA activity of the former. Further studies are therefore necessary to understand the role of H-bonding in the reactivity and spectroscopic properties of the non-heme oxoiron(IV) complexes, which are underway.

Acknowledgements

We are thankful to the Deutsche Forschungsgemeinschaft (DFG, German Research Foundation) under Germany's Excellence Strategy – EXC 2008-390540038 UniSysCat for the financial support. T.L. acknowledges support by the Deutsche Forschungsgemeinschaft (DFG, Project No. LO 2898/1-1). We thank the Helmholtz-Zentrum Berlin für Materialien und Energie for the allocation of synchrotron radiation beamtime. Open Access funding enabled and organized by Projekt DEAL.

Conflict of Interests

The authors declare no conflict of interest.

Data Availability Statement

The data that support the findings of this study are available in the supplementary material of this article.

Keywords: Bioinorganic chemistry · Metalloenzymes · Hydrogen bonds · Cyclam · Spectroscopy

[1] a) M. Costas, M. P. Mehn, M. P. Jensen, L. Que, *Chem. Rev.* **2004**, *104*, 939–986; b) E. I. Solomon, T. C. Brunold, M. I. Davis, J. N. Kemsley, S.-K. Lee, N. Lehnert, F. Neese, A. J. Skulan, Y.-S. Yang, J. Zhou, *Chem. Rev.s* **2000**, *100*, 235–350; c) M. Sono, M. P. Roach, E. D. Coulter, J. H. Dawson, *Chem. Rev.* **1996**, *96*, 2841–2888; d) B. J. Wallar, J. D. Lipscomb, *Chem. Rev.* **1996**, *96*, 2625–2658

[2] a) K. D. Koehntop, J. P. Emerson, L. Que, *JBIC J Biol. Inorg.Chem.* **2005**, *10*, 87–93. b) I. Monte Pérez, X. Engelmann, Y.-M. Lee, M. Yoo, E. Kumaran, E. R. Farquhar, E. Bill, J. England, W. Nam, M. Swart, K. Ray, *Angewandte Chemie Int. Ed.* **2017**, *56*, 14384–14388; c) X. Engelmann, D. D. Malik, T. Corona, K. Warm, E. R. Farquhar, M. Swart, W. Nam, K. Ray, *Angewandte Chemie Int. Ed* **2019**, *58*, 4012–4016; d) M. Guo, T. Corona, K. Ray, W. Nam, *ACS Central Sci.* **2019**, *5*, 13–28; e) P. Comba, A.-M. Löhr, F. Pfaff, K. Ray, *Israel J Chem.* **2020**, *60*, 957–962; f) D. Kass, T. Corona, K. Warm, B. Braun-Cula, U. Kuhlmann, E. Bill, S. Mebs, M. Swart, H. Dau, M. Haumann, P. Hildebrandt, K. Ray, *J Am. Chem. Soc.* **2020**, *142*, 5924–5928; g) V. A. Larson, B. Battistella, K. Ray, N. Lehnert, W. Nam, *Nature Rev. Chem.* **2020**, *4*, 404–419; h) X.-P. Zhang, A. Chandra, Y.-M. Lee, R. Cao, K. Ray, W. Nam, *Chem. Soc. Rev.* **2021**, *50*, 4804–4811.

[3] a) A. Decker, J.-U. Rohde, E. J. Klinker, S. D. Wong, L. Que, E. I. Solomon, *J Am. Chem. Soc.* **2007**, *129*, 15983–15996; b) X. Engelmann, I. Monte-Pérez, K. Ray, *Angewandte Chemie Int. Ed.* **2016**, *55*, 7632–7649; c) J. England, M. Martinho, E. R. Farquhar, J. R. Frisch, E. L. Bominaar, E. Münck, L. Que Jr, *Angewandte Chemie Int. Ed.* **2009**, *48*, 3622–3626; d) J. Hohenberger, K. Ray, K. Meyer, *Nature Commun.* **2012**, *3*, 720; e) D. C. Lacy, R. Gupta, K. L. Stone, J. Greaves, J. W. Ziller, M. P. Hendrich, A. S. Borovik, *J Am. Chem. Soc.* **2010**, *132*, 12188–12190; f) A. R. McDonald, L. Que, *Coord. Chem. Rev.* **2013**, *257*, 414–428; g) W. Nam, *Accounts of Chemical Research* **2007**, *40*, 522–531; h) L. Que, Jr., *Acc. Chem. Res.* **2007**, *40*, 493–500; i) K. Ray, F. Heims, M. Schwalbe, W. Nam, *Curr. Opin. Chem. Biol.* **2015**, *25*, 159–171; j) K. Ray, F. F. Pfaff, B. Wang, W. Nam, *J Am. Chem. Soc* **2014**, *136*, 13942–13958; k) Y. Zang, J. Kim, Y. Dong, E. C. Wilkinson, E. H. Appelman, L. Que, *J Am. Chem. Soc.* **1997**, *119*, 4197–4205.

[4] a) J. M. Bollinger Jr, J. C. Price, L. M. Hoffart, E. W. Barr, C. Krebs, *Euro. J Inorg. Chem.* **2005**, *2005*, 4245–4254; b) B. E. Eser, E. W. Barr, P. A. Frantom, L. Saleh, J. M. Bollinger, Jr., C. Krebs, P. F. Fitzpatrick, *J Am. Chem. Soc.* **2007**, *129*, 11334–11335; c) D. P. Galonić, E. W. Barr, C. T. Walsh, J. M. Bollinger, C. Krebs, *Nature Chem. Biol.* **2007**, *3*, 113–116; d) L. M. Hoffart, E. W. Barr, R. B. Guyer, J. M. Bollinger, C. Krebs, *Proc. National Acad. Sci.* **2006**, *103*, 14738–14743; e) M. L. Matthews, C. M. Krest, E. W. Barr, F. H. Vaillancourt, C. T. Walsh, M. T. Green, C. Krebs, J. M. Bollinger, Jr., *Biochemistry* **2009**, *48*, 4331–4343; f) J. C. Price, E. W. Barr, B. Tirupati, J. M. Bollinger, C. Krebs, *Biochemistry* **2003**, *42*, 7497–7508.

[5] a) M. P. Jensen, M. Costas, R. Y. N. Ho, J. Kaizer, A. Mairata i Payeras, E. Münck, L. Que, J.-U. Rohde, A. Stubna, *J Am. Chem. Soc.* **2005**, *127*, 10512–10525; b) J. Kaizer, M. Costas, L. Que Jr, *Angewandte Chemie Int. Ed.* **2003**, *42*, 3671–3673; c) E. J. Klinker, J. Kaizer, W. W. Brennessel, N. L. Woodrum, C. J. Cramer, L. Que Jr, *Angewandte Chemie Int. Ed.* **2005**, *44*, 3690–3694.

[6] D. Wang, K. Ray, M. J. Collins, E. R. Farquhar, J. R. Frisch, L. Gómez, T. A. Jackson, M. Kerscher, A. Waleska, P. Comba, M. Costas, L. Que, *Chem. Sci.* **2013**, *4*, 282–291.

[7] a) M. R. Anneser, G. R. Elpitiya, J. Townsend, E. J. Johnson, X. B. Powers, J. F. DeJesus, K. D. Vogiatzis, D. M. Jenkins, *Angewandte Chemie Int. Ed.* **2019**, *58*, 8115–8118; b) F. G. Cantú Reinhard, S. P. De Visser, *Chemistry – A Euro. J* **2017**, *23*, 2935–2944; c) J. F. DeJesus, D. M. Jenkins, *Chemistry – A Euro. J* **2020**, *26*, 1429–1435; d) L. Gravogl, D. Kass, O. Pyschny, F. W. Heinemann, M. Haumann, S. Katz, P. Hildebrandt, H. Dau, A. Swain, R. García-Serres, K. Ray, D. Munz, K. Meyer, *J Am. Chem. Soc.* **2024**; e) H. Kropp, A. E. King, M. M. Khusniyarov, F. W. Heinemann, K. M. Lancaster, S. DeBeer, E. Bill, K. Meyer, *J Am. Chem. Soc.* **2012**, *134*, 15538–15544; f) C. Kupper, B. Mondal, J. Serrano-Plana, I. Klawitter, F. Neese, M. Costas, S. Ye, F. Meyer, *J Am. Chem. Soc.* **2017**, *139*, 8939–8949; g) J. J. Scepaniak, C. S. Vogel, M. M. Khusniyarov, F. W. Heinemann, K. Meyer, J. M. Smith, *Science* **2011**, *331*, 1049–1052.

[8] a) M. Srnec, S. D. Wong, J. England, L. Que, E. I. Solomon, *Proc. National Acad. Sci.* **2012**, *109*, 14326–14331; b) S.-C. Chan, P. Gupta, X. Engelmann, Z. Z. Ang, R. Ganguly, E. Bill, K. Ray, S. Ye, J. England, *Angewandte Chemie Int. Ed.* **2018**, *57*, 15717–15722; c) A. B. Jacobs, R.

Banerjee, D. E. Deweese, A. Braun, J. T. Babicz, L. B. Gee, K. D. Sutherlin, L. H. Böttger, Y. Yoda, M. Saito, S. Kitao, Y. Kobayashi, M. Seto, K. Tamasaku, J. D. Lipscomb, K. Park, E. I. Solomon, *J Am. Chem. Soc.* **2021**, *143*, 16007–16029; d) T. Kroll, M. L. Baker, S. A. Wilson, M. Lundberg, A. Juhin, M.-A. Arrio, J. J. Yan, L. B. Gee, A. Braun, T.-C. Weng, D. Sokaras, B. Hedman, K. O. Hodgson, E. I. Solomon, *J Am. Chem. Soc.* **2021**, *143*, 4569–4584; e) E. I. Solomon, D. E. DeWeese, J. T. Babicz, *Biochemistry* **2021**, *60*, 3497–3506; f) J. T. Babicz, M. S. Rogers, D. E. DeWeese, K. D. Sutherlin, R. Banerjee, L. H. Böttger, Y. Yoda, N. Nagasawa, M. Saito, S. Kitao, M. Kurokuzu, Y. Kobayashi, K. Tamasaku, M. Seto, J. D. Lipscomb, E. I. Solomon, *J Am. Chem. Soc.* **2023**, *145*, 15230–15250; g) A. Braun, L. B. Gee, M. W. Mara, E. A. Hill, T. Kroll, D. Nordlund, D. Sokaras, P. Glatzel, B. Hedman, K. O. Hodgson, A. S. Borovik, M. L. Baker, E. I. Solomon, *J Am. Chem. Soc.* **2023**, *145*, 18977–18991; h) M. L. Bols, J. Ma, F. Rammal, D. Plessers, X. Wu, S. Navarro-Jaén, A. J. Heyer, B. F. Sels, E. I. Solomon, R. A. Schoonheydt, *Chem. Rev.* **2024**, *124*, 2352–2418; i) E. I. Solomon, R. R. Gipson, in *Methods in Enzymology, Vol. 703* (Ed.: J. Bridwell-Rabb), Academic Press, **2024**, pp. 29–49.

[9] T. A. Jackson, J.-U. Rohde, M. S. Seo, C. V. Sastri, R. DeHont, A. Stubna, T. Ohta, T. Kitagawa, E. Münck, W. Nam, L. Que, *J Am. Chem. Soc.* **2008**, *130*, 12394–12407.

[10] a) D. Mandal, R. Ramanan, D. Usharani, D. Janardanan, B. Wang, S. Shaik *J Am. Chem. Soc.* **2015**, *137*, 722–733; b) S. A. Wilson, J. Chen, S. Hong, Y.-M. Lee, M. Clémancey, R. Garcia-Serres, T. Nomura, T. Ogura, J.-M. Latour, B. Hedman, K. O. Hodgson, W. Nam, E. I. Solomon, *J Am. Chem. Soc.* **2012**, *134*, 11791–11806.

[11] S. Shaik, H. Chen, D. Janardanan, *Nature Chem.* **2011**, *3*, 19–27.

[12] a) H. Hirao, L. Que Jr, W. Nam, S. Shaik, *Chemistry – A Euro. J* **2008**, *14*, 1740–1756; b) E. J. Klinker, S. Shaik, H. Hirao, L. Que Jr, *Angewandte Chemie International Edition* **2009**, *48*, 1291–1295; c) D. B. Rice, D. Wong, T. Weyhermüller, F. Neese, S. DeBeer, *Sci. Advances*, *10*.

[13] C. V. Sastri, J. Lee, K. Oh, Y. J. Lee, J. Lee, T. A. Jackson, K. Ray, H. Hirao, W. Shin, J. A. Halfen, J. Kim, L. Que, S. Shaik, W. Nam, *Proc. National Acad. Sci.* **2007**, *104*, 19181–19186.

[14] T. Devi, K. Dutta, J. Deutscher, S. Mebs, U. Kuhlmann, M. Haumann, B. Cula, H. Dau, P. Hildebrandt, K. Ray, *Chem. Sci.* **2024**, *15*, 528–533.

[15] a) Z. Gross, S. Nimri, *Inorg. Chem.* **1994**, *33*, 1731–1732; b) K. L. Stone, R. K. Behan, M. T. Green, *Proc. National Acad. Sci.* **2005**, *102*, 16563–16565; c) J. A. Kovacs, L. M. Brines, *Acc. Chem. Res.* **2007**, *40*, 501–509; d) M. T. Green, *Curr. Opin. Chem. Biol.* **2009**, *13*, 84–88; e) C. M. Krest, A. Silakov, J. Rittle, T. H. Yosca, E. L. Onderko, J. C. Calixto, M. T. Green, *Nature Chem.* **2015**, *7*, 696–702; f) T. H. Yosca, M. C. Langston, C. M. Krest, E. L. Onderko, T. L. Grove, J. Livada, M. T. Green, *J Am. Chem. Soc.* **2016**, *138*, 16016–16023; g) T. H. Yosca, A. P. Ledray, J. Ngo, M. T. Green, *JBIC J Biol. Inorg. Chem.* **2017**, *22*, 209–220; h) K. Mittra, M. T. Green, *J Am. Chem. Soc.* **2019**, *141*, 5504–5510; i) A. P. Ledray, C. M. Krest, T. H. Yosca, K. Mittra, M. T. Green, *J Am. Chem. Soc* **2020**, *142*, 20419–20425.

[16] a) S. M. Barry, G. L. Challis, *ACS Catalysis* **2013**, *3*, 2362–2370; b) D. J. Ferraro, L. Gakhar, S. Ramaswamy, *Biochem. Biophys. Res. Commun.* **2005**, *338*, 175–190; c) M. D. White, E. Flashman, *Curr. Opin. Chem. Biol.* **2016**, *31*, 126–135.

[17] D. M. I. Bandara, M. Sono, G. S. Bruce, A. R. Brash, J. H. Dawson, *J Inorg. Biochem.* **2011**, *105*, 1786–1794.

[18] K. Ray, J. England, A. T. Fiedler, M. Martinho, E. Münck, *Angewandte Chemie Int. Edition* **2008**, *47*, 8068–8071.

[19] N. AlHaddad, E. Lelong, J.-M. Suh, M. Cordier, M. H. Lim, G. Royal, C. Platas-Iglesias, H. Bernard, R. Tripier, *Dalton Transactions* **2022**, *51*, 8640–8656.

[20] a) A. G. Blackman, E. B. Schenk, R. E. Jelley, E. H. Krenske, L. R. Gahan, *Dalton Transactions* **2020**, *49*, 14798–14806; b) A. W. Addison, T. N. Rao, J. Reedijk, J. van Rijn, G. C. Verschoor, *J Chem. Soc., Dalton Trans.* **1984**, 1349–1356.

[21] B. Bosnich, C. K. Poon, M. L. Tobe, *Inorg. Chem.* **1965**, *4*, 1102–1108.

[22] a) J.-U. Rohde, J.-H. In, M. H. Lim, W. W. Brennessel, M. R. Bukowski, A. Stubna, E. Münck, W. Nam, L. Que, *Science* **2003**, *299*, 1037–1039; b) A. T. Fiedler, H. L. Halfen, J. A. Halfen, T. C. Brunold, *J Am. Chem. Soc.* **2005**, *127*, 1675–1689; c) C. V. Sastri, M. J. Park, T. Ohta, T. A. Jackson, A. Stubna, M. S. Seo, J. Lee, J. Kim, T. Kitagawa, E. Münck, L. Que, W. Nam, *J Am. Chem. Soc.* **2005**, *127*, 12494–12495; d) S. Fukuzumi, Y. Morimoto, H. Kotani, P. Naumov, Y.-M. Lee, W. Nam, *Nature Chem.* **2010**, *2*, 756–759; e) A. R. McDonald, M. R. Bukowski, E. R. Farquhar, T. A. Jackson, K. D. Koehntop, M. S. Seo, R. F. De Hont, A. Stubna, J. A. Halfen, E. Münck, W. Nam, L. Que, Jr., *J Am. Chem. Soc.* **2010**, *132*, 17118–17129; f) J. Cho, S. Jeon, S. A. Wilson, L. V. Liu, E. A. Kang, J. J. Braymer, M. H. Lim, B. Hedman, K. O. Hodgson, J. S. Valentine, E. I. Solomon, W. Nam, *Nature* **2011**, *478*, 502–505; g) J. Prakash, G. T. Rohde, K. K. Meier, A. J. Jasniewski, K. M. Van Heuvelen, E. Münck, L. Que, Jr., *J Am. Chem. Soc.* **2015**, *137*, 3478–3481; h) M. R. Bukowski, K. D. Koehntop, A. Stubna, E. L. Bominaar, J. A. Halfen, E. Münck, W. Nam, L. Que, *Science* **2005**, *310*, 1000–1002.

[23] J. England, J. O. Bigelow, K. M. Van Heuvelen, E. R. Farquhar, M. Martinho, K. K. Meier, J. R. Frisch, E. Münck, L. Que, *Chem. Sci.* **2014**, *5*, 1204–1215.

[24] a) J. Prakash, G. T. Rohde, K. K. Meier, E. Münck, L. Que, Jr., *Inorg. Chem.* **2015**, *54*, 11055–11057; b) J. Prakash, Y. Sheng, A. Draksharapu, J. E. M. N. Klein, C. J. Cramer, L. Que Jr, *Angewandte Chemie International Edition* **2019**, *58*, 1995–1999; c) B. Chandra, F. Ahsan, Y. Sheng, M. Swart, L. Que, *Proceedings of the National Academy of Sciences* **2024**, *121*, e2319799121; d) To generate **1-*syn*** in deprotonated state, 1.2 equivalent of triethylamine was added to the starting complex, $[Fe^{II}(TMC\text{-}HOR)]^{2+}$ and the reaction mixture was stirred for 15 minutes at room temperature. Then 1.2 equivalent sPhIO was added at −40 °C. At this stage, no change in the NIR region was observed. Even after adding 1.2 equivalent of $HClO_4$, at −40 °C **1-*syn*** couldn't be generated as confirmed from no change in the NIR region (See ESI, Figure S3 for UV-vis spectra); e) R. Hooke, *Lectures de Potentia Restitutiva, Or of Spring Explaining the Power of Springing Bodies*, John Martyn, **1678**.

[25] a) E. A. Hill, A. C. Weitz, E. Onderko, A. Romero-Rivera, Y. Guo, M. Swart, E. L. Bominaar, M. T. Green, M. P. Hendrich, D. C. Lacy, A. S. Borovik, *J Am. Chem. Soc.* **2016**, *138*, 13143–13146; b) A. C. Weitz, E. A. Hill, V. F. Oswald, E. L. Bominaar, A. S. Borovik, M. P. Hendrich, Y. Guo, *Angewandte Chemie Int. Ed.* **2018**, *57*, 16010–16014; c) S. K. Barman, J. R. Jones, C. Sun, E. A. Hill, J. W. Ziller, A. S. Borovik, *J Am. Chem. Soc.* **2019**, *141*, 11142–11150; d) V. F. Oswald, J. L. Lee, S. Biswas, A. C. Weitz, K. Mittra, R. Fan, J. Li, J. Zhao, M. Y. Hu, E. E. Alp, E. L. Bominaar, Y. Guo, M. T. Green, M. P. Hendrich, A. S. Borovik, *J Am. Chem. Soc.* **2020**, *142*, 11804–11817.

[26] a) Z. Gong, L. Wang, Y. Xu, D. Xie, X. Qi, W. Nam, M. Guo, *Adv. Sci.* **2024**, *11*, 2310333; b) M. A. Ehudin, L. B. Gee, S. Sabuncu, A. Braun, P. Moënne-Loccoz, B. Hedman, K. O. Hodgson, E. I. Solomon, K. D. Karlin, *J Am. Chem. Soc.* **2019**, *141*, 5942–5960.

[27] Deposition number **2406259** (for $[Fe^{II}(TMC\text{-}HOR)](CF_3SO_3)_2]$. CH_3CN) contain the supplementary crystallographic data for this paper. This data is provided free of charge by the joint Cambridge Crystallographic Data Centre and Fachinformationszentrum Karlsruhe Access Structures service.

[28] A. D. Cardenal, A. Maity, W.-Y. Gao, R. Ashirov, S.-M. Hyun, D. C. Powers, *Inorg. Chem.* **2019**, *58*, 10543–10553.

[29] K. S. Hagen, *Inorg. Chem.* **2000**, *39*, 5867–5869.

[30] a) F. Neese, *WIREs Comput. Mol. Sci.* **2012**, *2*, 73–78; b) F. Neese, F. Wennmohs, U. Becker, C. Riplinger, *J Chem. Phys.* **2020**, *152*, 224108; c) F. Neese, *WIREs Computational Molecular Science* **2022**, *12*, e1606; d) F. Neese, *J Comput. Chem.* **2023**, *44*, 381–396.

[31] a) J. P. Perdew, *Physical Review B* **1986**, *33*, 8822–8824; b) A. D. Becke, *Physical Review A* **1988**, *38*, 3098–3100.

[32] a) E. V. Lenthe, E. J. Baerends, J. G. Snijders, *J Chem. Physics* **1993**, *99*, 4597–4610; b) E. van Lenthe, E. J. Baerends, J. G. Snijders, *J Chem. Physics* **1994**, *101*, 9783–9792; c) C. van Wüllen, *J Chem. Physics* **1998**, *109*, 392–399.

[33] D. A. Pantazis, X.-Y. Chen, C. R. Landis, F. Neese, *J Chem. Theory and Comput.* **2008**, *4*, 908–919.

[34] F. Neese, *J Computat. Chem.* **2003**, *24*, 1740–1747.

[35] F. Weigend, *Phys. Chem. Chem. Physics* **2006**, *8*, 1057–1065.

[36] V. Barone, M. Cossi, *J Phys. Chem. A* **1998**, *102*, 1995–2001.

[37] a) S. Grimme, J. Antony, S. Ehrlich, H. Krieg, *J Chem. Physics* **2010**, *132*, 154104; b) S. Grimme, S. Ehrlich, L. Goerigk, *J Comput. Chem.* **2011**, *32*, 1456–1465.

Manuscript received: December 3, 2024
Accepted manuscript online: March 3, 2025
Version of record online: April 22, 2025